Model-based Design and Optimization of Passive Shoulder Exoskeletons

Ali Nasr
Department of Systems Design Engineering,
University of Waterloo,
Waterloo, ON N2L-3G1, Canada
Email: a.nasr@uwaterloo.ca

Spencer Ferguson
Department of Systems Design Engineering,
University of Waterloo,
Waterloo, ON N2L-3G1, Canada
Email: spencer.ferguson@uwaterloo.ca

John McPhee
Department of Systems Design Engineering,
University of Waterloo,
Waterloo, ON N2L-3G1, Canada
Email: mcphee@uwaterloo.ca

ABSTRACT

To physically assist workers in reducing musculoskeletal strain or to develop motor skills for patients with neuromuscular disabilities, recent research has focused on exoskeletons. Designing exoskeletons is challenging due to the complex human geometric structure, the human-exoskeleton wrench interaction, the kinematic constraints, and the selection of power source characteristics. This study concentrates on modeling a 3D multibody upper-limb human-exoskeleton, developing a procedure of analyzing optimal assistive torque profiles, and optimizing the passive mechanism features for desired tasks. The optimization objective is minimizing the human joint torques. Differential-algebraic equations (DAE)s of motion have been generated and solved to simulate the complex closed-loop multibody dynamics. Three different tasks have been considered, which are common in industrial environments: object manipulation, over-head work, and static pointing. The resulting assistive exoskeleton's elevation joint torque profile decreases the specific task's human shoulder torque in computer simulations. The exoskeleton is not versatile or optimal for different dynamic tasks since the passive mechanism produces a specific torque for a given elevation angle. We concluded that designing a fully passive exoskeleton for a wide range of dynamic applications is impossible.

1 Introduction

Musculoskeletal Disorder (MSD) cases account for 33% of all worker injury and disorder cases, with 22% of these MSDs affecting the upper extremity [1], making it one of the most common regional pain syndromes. To deal with the prevalence of MSDs in object handling tasks, as well as to assist in shoulder rehabilitation and

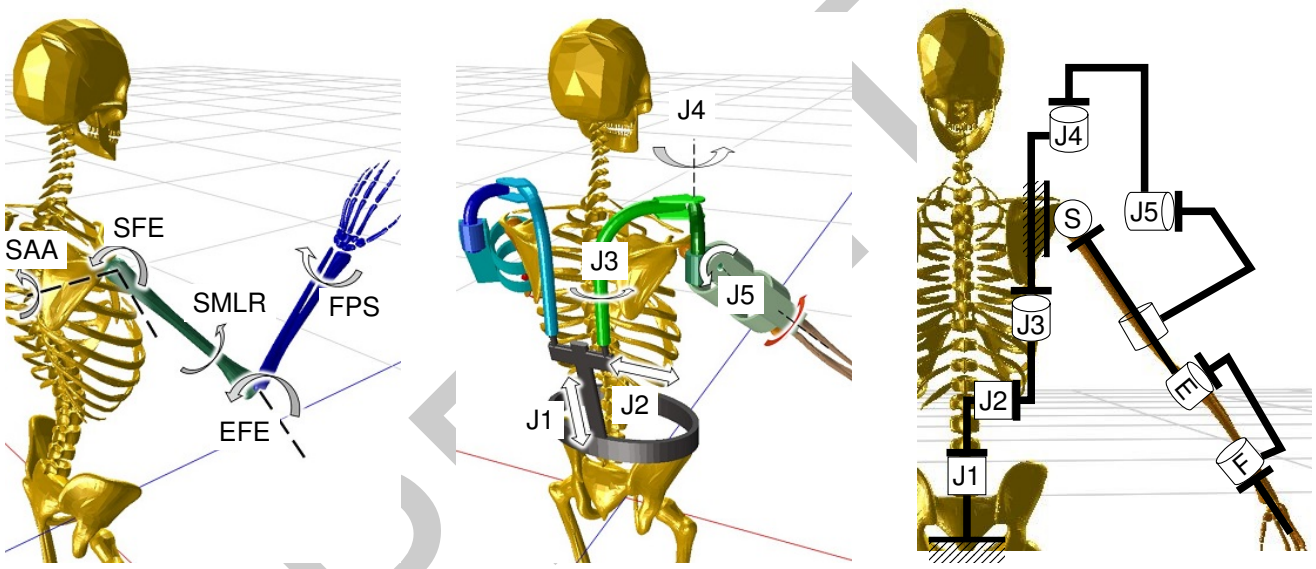

(a) Human Skeletal System (b) Exoskeleton's Body System (c) Human-exoskeleton Closed Chain

Fig. 1: (a) Schematic of the shoulder and elbow 5 DoF (SFE: Shoulder Flexion/Extension, SAA: Shoulder Abduction/Adduction, SMLR: Shoulder Medial/Lateral Rotation, EFE: Elbow Flexion/Extension, and FPS: Forearm Pronation/Supination). (b) Schematic of the 5 DoF of the airframe exoskeleton (J1. Vertical adjustment, J2. Horizontal adjustment, J3. Rotational adjustment, J4. Free internal/external rotation joint, and J5. Elevation joint). (c) Schematic of the human-exoskeleton (right side) closed kinematic chain system with ten joints, five DoF, and five constraints.

human-augmentation, research has focused on upper-limb exoskeletons [2, 3, 4, 5, 6], defined as mechanical structures that enhance users' strength. Exoskeletons have been designed to (I) physically assist workers and (II) recover or develop motor skills for patients in performing their tasks. In terms of assistance, these devices reduce the exposure to the associated physical demands and strain placed on the shoulders. Exoskeletons also have the potential to lessen perceived exertion, shoulder flexor muscle activity, and shoulder joint torque [2, 3, 6, 7].

In contrast to bulky nonportable exoskeletons with strong motors, portable and wearable devices can be used in various industrial and clinical environments. The source of exoskeletons' joint torque profiles is categorized as fully passive, fully active, and passive-active (semi-active or semi-passive). Fully passive exoskeletons use a mechanism that can only generate an assistive torque in the direction of flexion or abduction (which is a resistive torque in the direction of extension or adduction), or in other words, only have the capability of gravity-compensating [8]. Examples of Fully passive exoskeletons include the Airframe [9], SkelEx [10], LE SHIVA EXO [11], ShoulderX [12], EksoVest [13], and MATE [14]. These exoskeletons have a lower weight in comparison to fully active (motor-actuated) exoskeletons and have an inherent safety. However, passive devices are bounded to providing gravity balancing. Although fully active devices could provide flexible torque profiles, in comparison to fully passive exoskeletons, they require maintenance or repair, sophisticated equipment, have higher overall cost, and are more cumbersome (mass of battery, actuators, sensors, and control unit) [15].

According to Perry et al., who showed that the forces/torque due to gravitational effects are much more considerable than Coriolis, centrifugal, and inertial loads [16, 17], the passive mechanism can be designed for the

gravitational effects of upper-limbs with no external disturbance wrench (force or torque). Basically, to design exoskeletons, human upper-limb models, which kinematically constrain an exoskeleton, have been used to optimize different cost functions. Kinematics examples include: optimal dimensions and kinematic fit [18], motion optimization [19, 20, 21], or optimizing the link dimensions [22]. Dynamics examples include: the minimization of muscle forces [23], joint torque [20, 24], or energy consumption [25]. Specifically, in the optimization of a dynamic parameter (minimizing the muscle tension), inverse dynamic simulation of the model or the computed generalized torque or force control method is used for different tasks as a nonlinear optimization problem [23].

Regardless of the exoskeleton design challenges associated with the complicated human-exoskeleton interaction, the literature has not provided clear guidelines or procedures to design passive mechanism system features of wearable assistive upper-limb exoskeletons according to specific tasks to the best of our knowledge. This goal will be achieved using two identical optimization loops and using the differential-algebraic equations (DAE)s from a multibody model for the human-exoskeleton system. The optimization cost function is minimizing the user elevation effort (human shoulder torque). The main research contributions are the dynamic optimization framework, detailed passive mechanism design, and decreasing the required user torque. We have concluded with the recommendation of parallelly augmenting an actuator (motor) to the passive mechanism (semi-active or semi-passive), which has the benefit of both systems.

2 Modeling

In the first phase of model development, we modeled a 3D human skeletal upper-limb. Secondly, the model was enriched with a wearable shoulder exoskeleton, integrated with the human arm model. This closed-loop multibody model was used for the simulation, optimization, and assessment.

2.1 Upper-Limb Human Skeletal Model

The skeletal model is necessary for representing the human upper limb. The skeletal upper-extremity model should be built with a simple structure to be used in the optimization loop or control loop. Considering the robot performs 3D (spatial) movements, the skeletal arm was modeled as a 3D two-link arm.

We have initially considered the 3D Stanford VA skeletal arm model [26] without including the wrist joint. It allows 3 Degrees of Freedom (DoF) at the shoulder, 1 DoF at the elbow (flexion/extension), and 1 DoF for forearm pronation/supination. Consequently, the 3D skeletal arm model has 5 DoF.

In the 3D skeletal model, the shoulder joint is modeled by three revolute joints with intersecting axes (SFE: Shoulder Flexion/Extension, SAA: Shoulder Abduction/Adduction, SMLR: Shoulder Medial/Lateral Rotation) as shown in left section of Fig. 1. As depicted in 1, the elbow has 2 DoF of EFE: Elbow Flexion/Extension, and FPS: Forearm Pronation/Supination. The International Society of Biomechanics Standard [27] for the shoulder and elbow joints has been considered for defining the coordinates.

The body segment inertial parameters (BSIP) of the upper arm (humerus), forearm (ulna and radius), and

hand were taken from Dumas et al. [28].

2.2 Exoskeleton Model

The upper-extremity exoskeleton system is a wearable robot (middle of Fig. 1), which provides additional external torque for the shoulder joint. The Airframe [9], which is designed and developed by Levitate Technologies, Inc. (California, USA), is used as an exoskeleton example. The base of the exoskeleton is fixed to the human waist. As shown in middle of Fig. 1, the exoskeleton has five joints, 2 prismatic joints and 3 revolute joints: vertical adjustment (J1), horizontal adjustment (J2), rotational adjustment (J3), free internal/external rotation joint (J4), and elevation joint (J5). Specifically, the three adjustment links/joints (J1-3) are used to ensure the exoskeleton elevation joint center is near or coincident with the shoulder joint center [29]. The exoskeleton elevation joint (J5) has a passive mechanism designed for specific tasks in this research.

The exoskeleton cushion is connected to the upper arm segment with a 5 DoF constraint (3 forces and 2 torques). In other words, the exoskeleton's last body link is attached to the human upper-arm by a 1 DoF revolute joint with axis in the shoulder pronation/supination direction (shown in middle of Fig. 1). Once attached, the exoskeleton's elevation joint angles (J5) can be derived from human shoulder orientation using the kinematic constraint equations.

The upper-arms of the human and the exoskeleton are forced to rotate and move together, apart from the allowed 1 DOF of pronation/supination rotation. Since the exoskeleton should follow the shoulder rotation, the exoskeleton adopts the exact same location of the shoulder joint center. In other words, the connection of the human-exoskeleton at the upper-arm forces the exoskeleton elevation joint center to coincide with the human shoulder joint center. To achieve this, the adjustment DOFs (J1-3) assume the fixed values necessary to locate the exoskeleton elevation joint center at the corresponding point on the human shoulder.

2.3 Multibody Model

By using the Multibody Analysis module of MapleSim (Waterloo, ON, Canada), the symbolic motion equations of the integrated human-exoskeleton model were extracted as follows:

$$\mathbf{M}_{n\times n}\dot{\mathbf{p}}_{n\times 1}+\mathbf{C}^{T}_{m\times n}\boldsymbol{\lambda}_{m\times 1}-\mathbf{Q}_{n\times 1}=\mathbf{F}_{n\times 1} \tag{1}$$

$$\boldsymbol{\Phi}\left(\mathbf{q}_{n\times 1},t\right)_{m\times 1}=\mathbf{0}_{m\times 1} \tag{2}$$

$$\dot{\mathbf{q}}_{n\times 1}-\mathbf{h}\left(\mathbf{p}_{n\times 1},\mathbf{q}_{n\times 1},t\right)_{n\times 1}=\mathbf{0}_{n\times 1} \tag{3}$$

where $\mathbf{M}$ is the mass matrix, $\mathbf{F}$ is the right-hand side of the dynamic equations (except actuation torque/force), which consists of gravitational, Coriolis and centrifugal effects, $\boldsymbol{\lambda}$ are Lagrange multipliers that enforce the kinematic constraint equations, $\mathbf{C}$ is the Jacobian matrix of the velocity constraint equations with respect to the n

generalized speeds $\mathbf{p}$ or coefficient matrix of constraint reactions, $\mathbf{\Phi}$ is the position-level kinematic constraint equations in terms of *n* coordinates, and $\mathbf{h}$ is the right-hand side of the transformation between $\dot{\mathbf{q}}$ (the derivative of position) and $\mathbf{p}$ (velocity).

The generalized coordinates ($\mathbf{q}$) consist of human joints (shoulder, EFE, and EPS) and robot revolute or prismatic joints (J1, J2, J3, J4, and J5), both for the right and left side. Particularly, the spherical shoulder joint was defined by an X-Z-Y Euler representation. However, the velocity vector ($\mathbf{p}$) was defined according to the order of generalized coordinate variables but with SFE in the sagittal plane, SAA in the frontal plane, and SMLR representation for the shoulder joint. Explicitly, the joints' velocity is represented in the sagittal and frontal plane, but the joints' angle is defined in Euler angles. Thus, the derivative of the joint angle vector is not equal to velocity. The joint velocity is transformed to the derivative of the joint angle using Eqn. (3). Precisely, Eqn. (3) consists of $\mathbf{p} = \dot{\mathbf{q}}$ for single-DoF joints and $\mathbf{p} = [\omega_x, \omega_y, \omega_y]^T$ for the 3-DoF shoulder joint.

The dimension of *n* is 20 (10 joints for each side, which consists of 5 joints for each arm and 5 joints for each side of the exoskeleton), and *m* is the number of total constraints (10 in total: 5 for each arm-exoskeleton attachment constraint enforced by 3-forces and 2-torques). The mentioned 5 constraints (3 translational and 2 rotational constraints) are due to the revolute joint connection between the exoskeleton and the human.

Due to the structure of the Airframe's [9] joints, adjustments, and constraints, the intersection center of the exoskeleton's joint axes (abduction/adduction, elevation, and pronation/supination joint) are at the human shoulder joint axes intersection. Since the exoskeleton's adjustment joints axes are generally not co-axial with human joint axes, it is impossible to lump the exoskeleton's link mass with the human segmental body mass, and it is impossible to use ordinary differential equations (ODE)s. Because of the closed kinematic chains in the human-exoskeleton model (shown in the right section of Fig. 1), the governing equations are DAEs. If all the exoskeleton's joints coincide precisely with human joints, the exoskeleton's link/bodies can be lumped with human segmental bodies, and ODEs can be used [30].

2.4 Model Verification

Although this model does not include muscles, the upper-limb skeletal model has been verified by the data from Garner and Pandy [31]. For this validation, an inverse dynamic simulation for a specific motion has been performed. According to [31], for the same motion of a moving upper-limb, our model's magnitude follows the same pattern as the magnitude of torque from Garner and Pandy [31], Fig. 2.

3 Optimizing Design Parameters

The procedure consists of first designing a torque profile for the exoskeleton's elevation joint to decrease human torque, and secondly designing the mechanism's passive features. To this end, three different tasks have been considered: object manipulation (OM), over-head work (OHW), and static pointing (SP). The OM and OHW tasks have been depicted in the left section of Fig. 3.

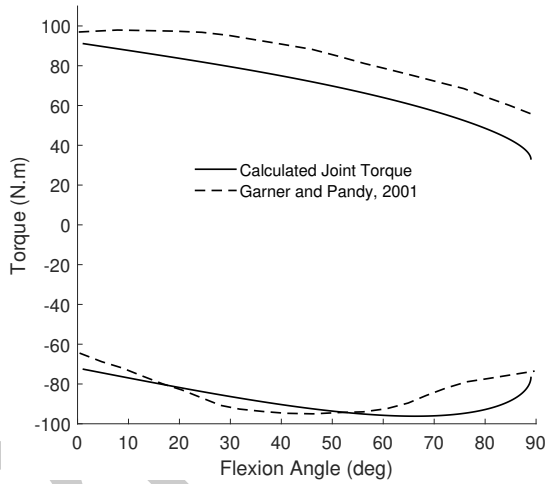

Fig. 2: Comparison of calculated joint torque with literature [31]. Flexion is positive, and extension is negative.

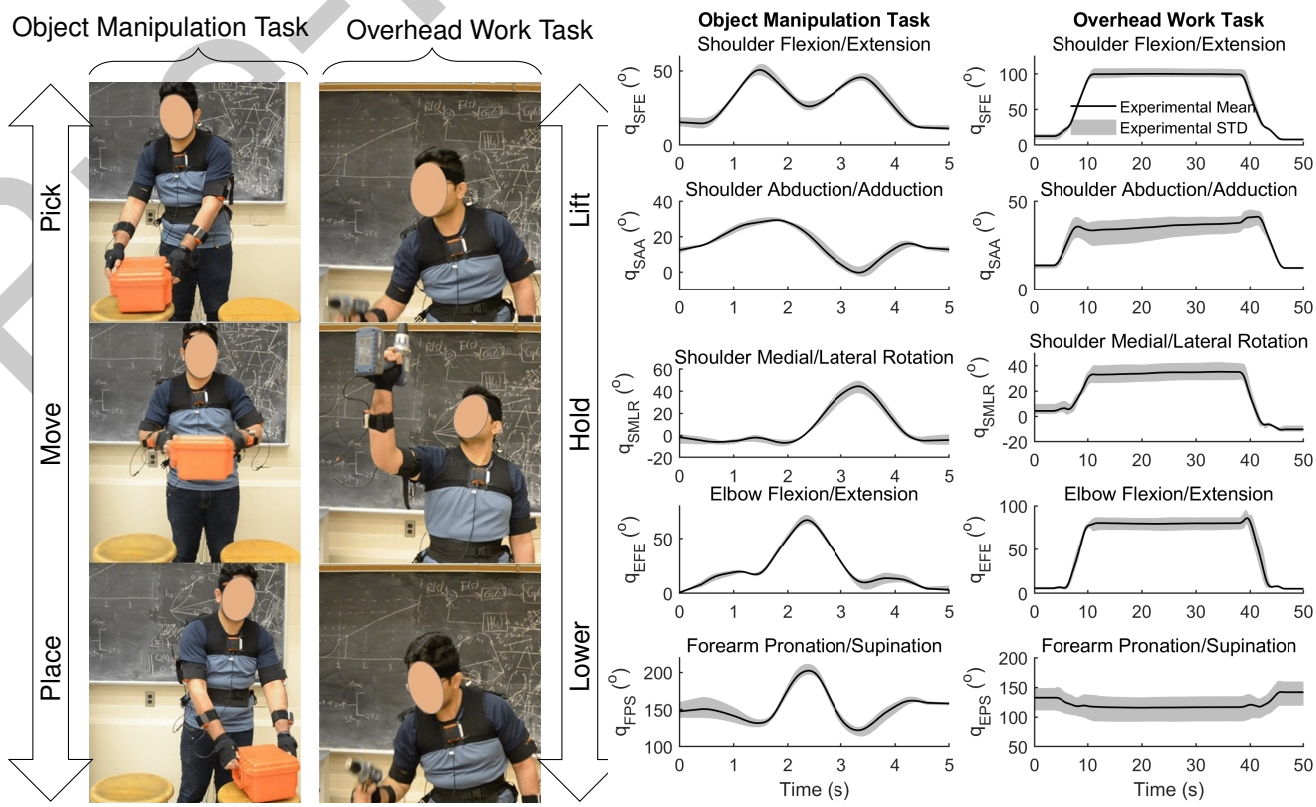

(a) Tasks

(b) Angular displacements

Fig. 3: (a) A depiction of the object manipulation (left) and overhead work (right) tasks performed for data collection. The participant lifted and lowered a weighted object between two target locations. (b) Relative angular displacements of the Shoulder Flexion/Extension (SFE), Shoulder Abduction/Adduction (SAA), Shoulder Medial/Lateral Rotation (SMLR), Elbow Flexion/Extension (EFE), and Forearm Pronation/Supination (FPS) throughout object manipulation (left), and over-head work task (right).

3.1 Experimental Motion

The angular human joint kinematics (without exoskeleton) were experimentally measured by the MVN Suit, Xsens Technologies, Netherlands [32] which is an inertial measurement unit (IMU) system. Following a standard calibration of the system, a subject performed two different tasks with 6 repetitions and 2 minutes of rest between tasks at the same time the joint kinematics were recorded with a sample rate of 100 Hz. The gimbal lock issue in the Euler sequence did not occur.

3.2 Kinematic Data Process

First of all, the measurements' high-frequency noise was reduced by a digital low-pass filter method using a 2nd order Butterworth filter with a 25 Hz cut-off frequency. Secondly, the torso's angles to the global and elbow joint axes were determined according to ISB recommendations, a Z-X-Y rotation sequence [27]. However, an X-Z-Y sequence (Plane Elevation, Elevation, Axial Rotation) was used for thoracohumeral angles [33], instead of the Y-X-Y recommended by ISB [27]. Thirdly, the joint angles were statistically evaluated using MATLAB. The average joint angle was computed and presented for OHW and OM tasks in the right section of Fig. 3. Then, the times for all tasks were scaled to the percentage completion of each task.

Using the human joint angles and using position constraints in Eqn. (2), the robot joint angles were calculated. Specifically, we have used a nonlinear system solver (f-solve) in MATLAB. Due to the nonlinear position constraints, sometimes, two different solutions for each configuration exist. Thus, we have added a memory to the position constraint. The result should have a minimum difference compared to previous steps.

Since the Euler representation has been used to define the shoulder joint's motion, the relation between the joint angle derivative and the joint angle's velocity is not linear, according to Eqn. (3). The joints' velocities were obtained first using the numerical first derivative of joint angles. Secondly, the position derivative was transformed to velocity using Eqn. (3).

Lastly, a digital low-pass filter method using a 2nd order Butterworth filter with a 20 Hz cut-off frequency was used to ignore the uncertainty of the computation of the velocity. The acceleration of joints was estimated by the numerical first derivative of joint velocities and a digital low-pass filter using a 2nd order Butterworth filter with a 30 Hz cut-off frequency.

3.3 Passive Mechanism Conceptual Design

We have designed the mechanism as provided in Fig. 4. The passive mechanism consists of Spring Stiffness k, Spring Initial Length L_0, Attachment Point $\vec{P}_A$, Wrap Point $\vec{P}_W$, and Base Point $\vec{P}_B$. The Attachment Point Position P_A can be defined by the Attachment Point Direction from the elevation joint and the gravity direction. The

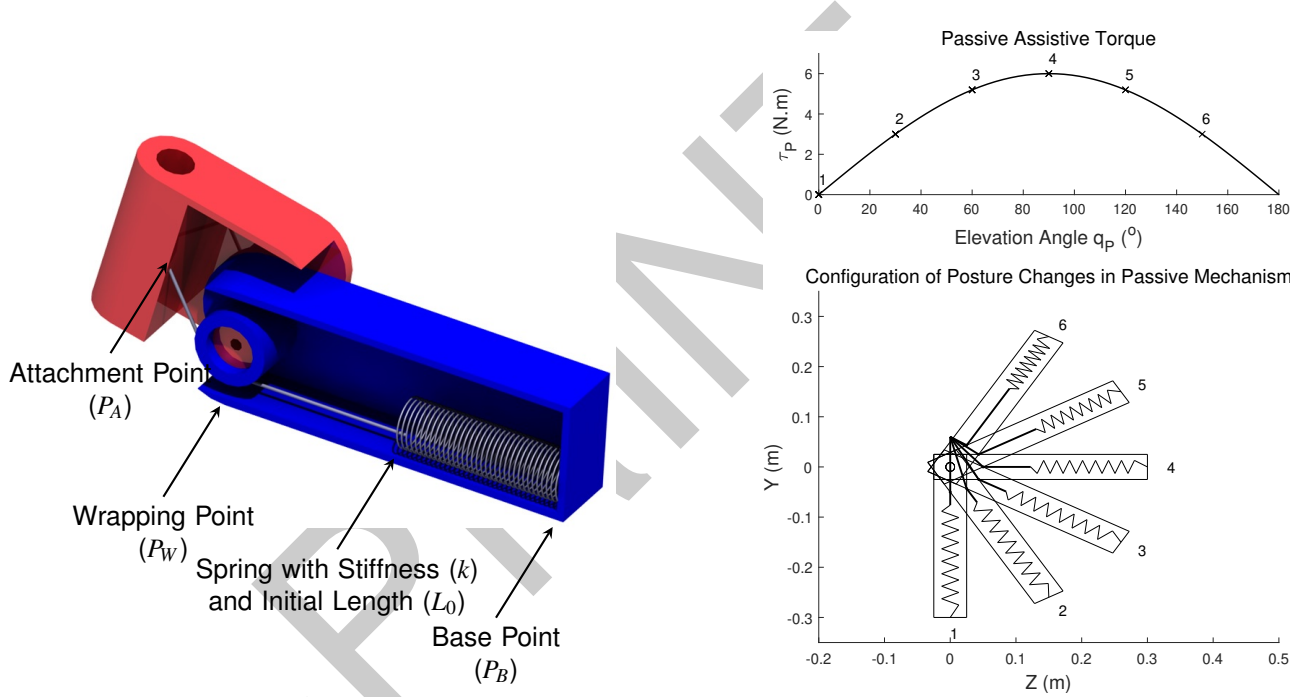

(a) (b)

Fig. 4: (a) A view of the passive elevation joint mechanism, consists of a spring, wrapping point, and revolute joint capable of producing the assistive torques. (b) A motion depiction of the passive elevation joint mechanism designed at different angles for the static pointing task.

mechanism assistive torque τ_p is as follows:

$$\vec{\tau}_p(\theta) = \vec{P}_A \times k \left[\frac{\vec{P}_A - \vec{P}_W}{\left|\vec{P}_A - \vec{P}_W\right|} \left(\left|\vec{P}_A + \vec{P}_B - 2\vec{P}_W\right| - L_0 \right) \right] \tag{4}$$

When the angle of the exoskeleton's elevation joint increases, the length of the spring decreases. Simultaneously, when the angle of the exoskeleton's elevation joint increases, the moment arm increases. The combination of decreasing the force of the spring (because of decreasing the length of spring) with increasing the moment arm of that force results in producing the required assistive torque. This mechanism is designed to produce a nonlinear torque-joint relationship thanks to the mechanism geometry, although the spring is linear.

3.4 Inverse Dynamic Simulation Background

For the given system motion (kinematics), the required forces and torques can be calculated with Eqn. (1), called inverse dynamic analysis. First, for a given prescribed motion, kinematic constraints (position, velocity, and acceleration) were solved using Eqn. (2). Secondly, Eqn. (1) was used for calculating reaction wrench $\boldsymbol{\lambda}$ and actuator wrench (force/torque) $\mathbf{Q}$.

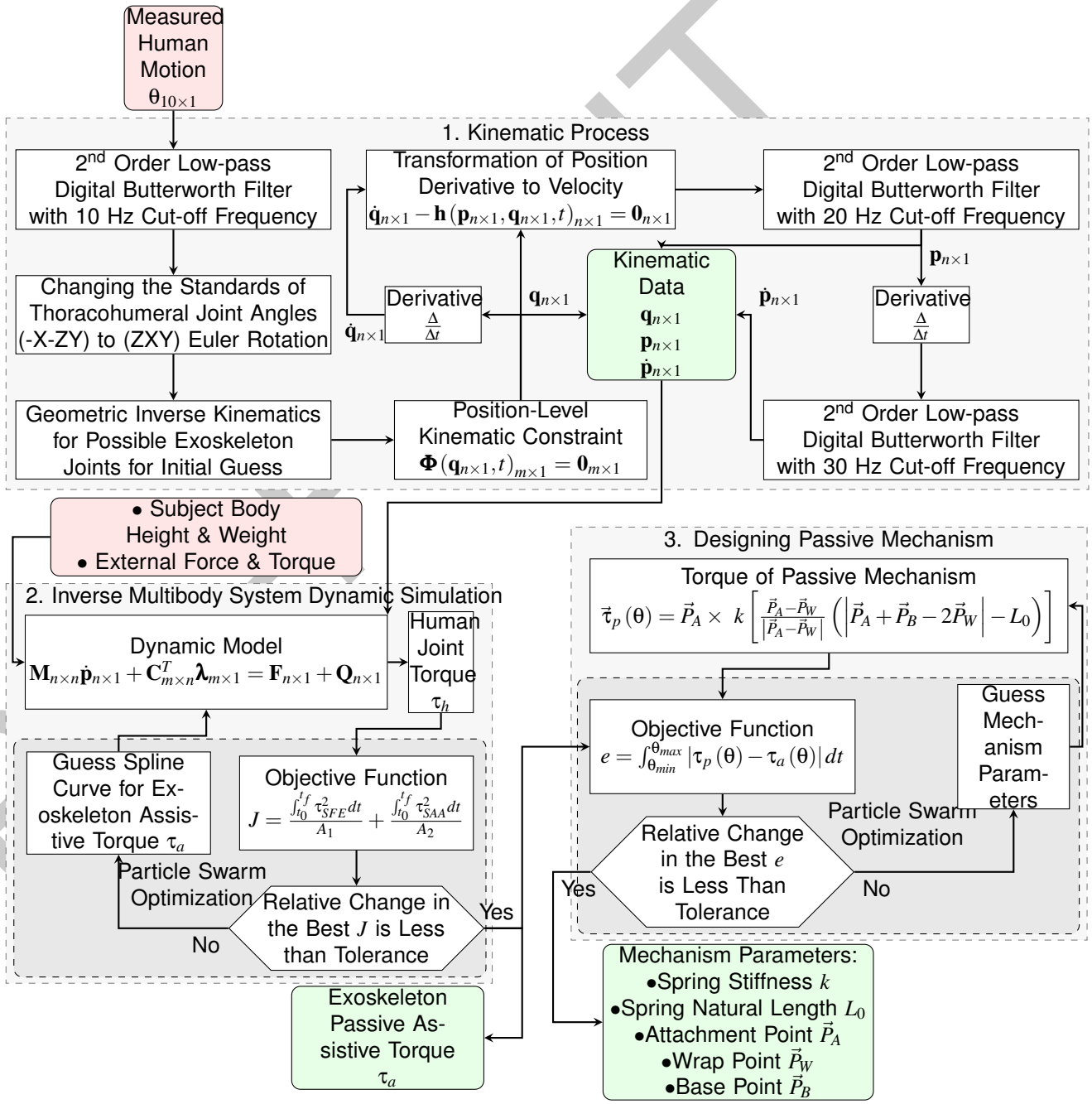

Fig. 5: The process of designing the passive joint mechanism with inverse dynamic simulation of the exoskeleton and skeletal system, by using a DAE-based nonlinear optimal control approach.

3.5 Optimal Design of Torque Profile

Fundamentally, decreasing the amount of torque in each joint or tension in each muscle is the goal of using an assistive robotic device. For the shoulder exoskeleton, the goal is to decrease the torque amount required to move the upper limb. Primarily, an assistive torque profile produced by the passive joint of the exoskeleton should be defined. Thus, minimizing the amount of torque demanded by the shoulder joint is a design requirement. We

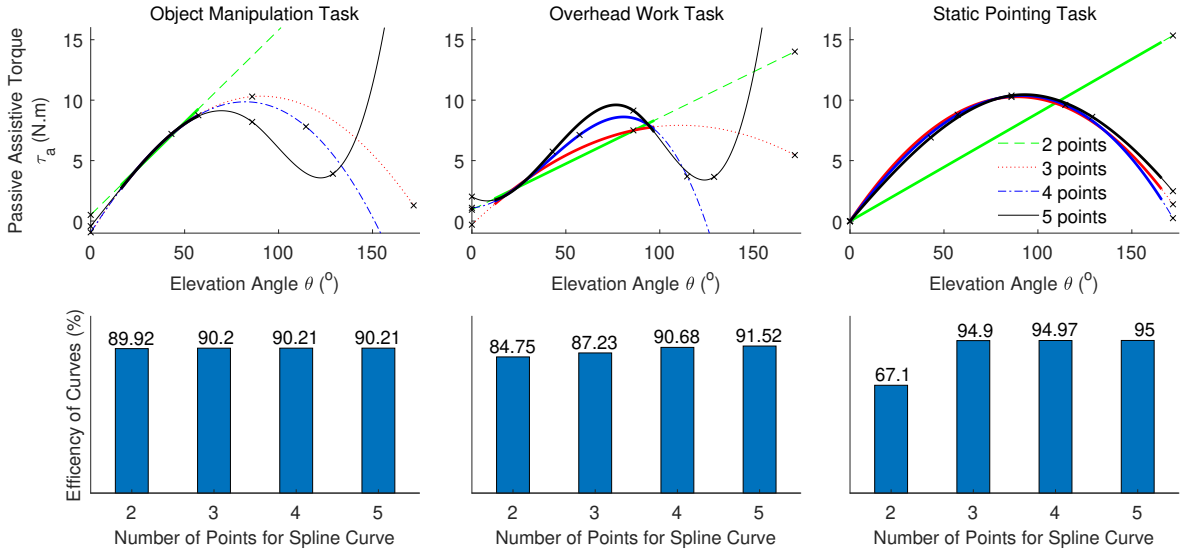

Fig. 6: Optimized passive joint torque profile with 2-5 points (top row), during object manipulation (left), over-head work (middle), and static pointing task (right) with efficiency (bottom row).

have used Eqn. (5) as the cost function for design optimization shown in Fig. 5.

$$J = \frac{\int_{t_0}^{t_f} \tau_{SFE}^2 dt}{A_1} + \frac{\int_{t_0}^{t_f} \tau_{SAA}^2 dt}{A_2} \tag{5}$$

where τ_{SFE} and τ_{SAA} are flexion/extension and abduction/adduction shoulder torque, respectively. A_1 and A_2 are the values of the relevant numerator when the exoskeleton is off and not producing any torque. Specifically, A_1 is equal to $\int_{t_0}^{t_f} \tau_{SFE}^2 dt$ when the exoskeleton is not applying any assistive torque. Similarly, A_2 is the value of $\int_{t_0}^{t_f} \tau_{SAA}^2 dt$ when the exoskeleton is not applying any assistive torque. Hence, we have divided the new situation (using assistive torque) by the common situation (not using assistive torque) to normalize the cost function. Minimizing the cost function in equation (5) decreases the elevation effort consisting of flexion and abduction torques that must work against the gravitational effects.

The particle swarm optimization method has been used to search different design variable values (points of polynomials function) to minimize the cost function. Specifically, the passive torque profiles may be linear, second-order, third-order, or fourth-order polynomial function of joint angle with 2, 3, 4, and 5 points, respectively. These 2, 3, 4, and 5 points are design parameters, and defined by the particle swarm optimization method (with a minimum of 100 particles in the swarm). The optimization loop is shown in Fig. 5.

The design variable value is the torque of exoskeleton's passive joint (the elevation joint). It is essential to mention that the passive joint of the exoskeleton is not a function of time since it consists of a conventional spring mechanism. The length of spring changes based on the exoskeleton's elevation joint angle. Thus, the torque

profile of exoskeleton's passive joint is a function of the joint angle.

3.6 Designing Passive Features

Using the best result of the optimization for passive torque profiles, we aim to design exoskeleton's passive joint mechanism. This goal has been achieved using the bottom loop in Fig. 5. This loop identifies the passive mechanism features to minimize the cost function in Eqn. (6), which represents the difference between the produced torque and the desired torque, whose profile was defined by the previous optimization loop. In solving this optimization problem, we have used the particle swarm optimization algorithm in MATLAB.

$$e = \int_{\theta_{min}}^{\theta_{max}} |\tau_p(\theta) - \tau_a(\theta)|\, dt \tag{6}$$

4 Results and Discussion

The result of the optimization for each polynomial is provided in Fig. 6. The top row of Fig. 6 is related to torque profile as a function of exoskeleton elevation joint angle. The bottom row of Fig. 6 is the comparison of the efficiency of each polynomial. The efficiency was calculated using Eqn. (7) where $\eta = 100$ means that the exoskeleton provides 100% of the torque required for a task.

$$\eta = \left[1 - \left(\frac{\int_{t_0}^{t_f} \tau_{SFE}^2 dt}{A_1} + \frac{\int_{t_0}^{t_f} \tau_{SAA}^2 dt}{A_2}\right)\right] \times 100 \tag{7}$$

By evaluating the provided torque in Fig. 6, it can be found that third-order curves (4 points) and fourth-order curves (5 points) are similar, meaning higher-order polynomial curves are not necessary. Thus, the passive torque profile with third-order curves (4 points) provides exoskeleton's elevation joint assistive torque to decrease the human shoulder torque.

The optimized passive joint torque profile with 2-5 points during object manipulation (top), overhead work (middle), and static pointing (bottom) tasks have been shown in the left column of Fig. 6. The torque profile line for the range of motion is bolder in Fig. 6 and evaluated for the specific task range. As shown in the left column of Fig. 6, the torque profiles for different tasks are not the same since the external force/torque is different. Thus, for each task, a specific assistive torque profile and, consequently, specific passive mechanism features are necessary.

This exoskeleton has been experimentally tested for tasks of bolting and tracing at two heights for four exoskeleton conditions [34]. The experimental results showed that that using an exoskeleton decreased feelings of effort and pain, although not much [34], which validated these computational results.

Fig. 4 shows the passive joint mechanism designed at different angles for the static pointing task. As an

example, for the static pointing task, Spring Stiffness k is 2000 (N/m), Spring Initial length L_0 is 0.250 (m), and Attachment Point Direction P_A is π (rad). However, the Spring Stiffness is much higher for the overwork task due to external force (object weight). The Attachment Point Direction for object manipulation (OM) task is different from the two others.

Based on the mechanical design, which has been provided in Fig. 4, the passive exoskeleton mechanism relies on kinetic energy and human strength to store energy in the spring mechanism. In other words, the spring mechanism uses the human strength or gravitational torque to store energy by lengthening the spring. The three passive torque profiles for the three tasks are different since the trajectory and the external loads are different. Designing a passive exoskeleton that can be used for different situations is not possible. The passive exoskeleton is designed only for one specific motion path and external force/torque profile. Suppose the upper-limb dynamics are changed by the manipulation of a different mass or different motion. In that case, the passive exoskeleton is no longer optimal. Even for OM, it is impossible to have an assistive exoskeleton which can be used for OM since there are different phases like object picking, object manipulation, and object release. Thus, the application of the passive exoskeleton is restricted by the work tasks and flexibility.

In contrast, fully active exoskeletons can provide significant advantages. They offer various torque profiles with Human-in-Loop (HIL) control, unlike passive mechanical mechanisms which provide constant assistance, with spring mechanisms requiring manual pre-stress settings. However, active devices are more cumbersome than passive exoskeletons (mass of battery, actuators, sensors, and control unit) and require maintaining or repairing sophisticated equipment, increasing the overall cost.

A possible solution to the mentioned problems may be a combination of a passive and active (semi-active or semi-passive) exoskeleton. According to Perry et al. [16, 17], the passive mechanism can be designed for the upper limb's gravitational effects with no external disturbance wrench like the manipulated object. Thus, the passive mechanism is designed for compensating the gravity torque of the upper limb. Meanwhile, an actuator provides extra torque for the rest of the required torque, relevant to radius-ulna, hand, and object reaction torque. In that case, the combination may assist humans in different situations. However, the main challenge is controlling the active part. Since the force/torque sensor might be heavy and bulky, knowing humans' intention for the motion is the solution for volitional control. A possible solution is using electromyography-based control and using muscle models [35, 36, 37, 38, 39].

5 Conclusion

In this study, a passive exoskeleton's mechanism has been designed. The study has focused on modeling a 3D upper-limb human-exoskeleton multibody system, developing a process of analyzing optimal assistive torque profiles, and optimizing the passive mechanism elements for desired tasks. Minimizing the human joint torques was the optimization cost function. Differential-algebraic equations have been used for simulating the complex multibody dynamics of the human-exoskeleton system. The passive exoskeleton has been designed for

three different tasks of object manipulation, over-head work, and static pointing. Although the resulting assistive exoskeleton's elevation torque profile could decrease the specific task's human shoulder torque, it was not a versatile torque profile and not optimal for different dynamic tasks. We proposed that augmenting an actuator to the mechanism can provide additional assistive torque.

Acknowledgements

This research is supported by funding from the Canada Research Chairs Program and the Natural Sciences and Engineering Research Council of Canada.

References

[1] Luime, J. J., Koes, B. W., Hendriksen, I. J., Burdorf, A., Verhagen, A. P., Miedema, H. S., and Verhaar, J. A., 2004. "Prevalence and incidence of shoulder pain in the general population; A systematic review". *Scandinavian Journal of Rheumatology,* **33**(2), pp. 73–81.

[2] Tahmid, S., Yang, J., and Font-Llagunes, J. M., 2019. "Review of models and robotic devices for stroke survivors' upper extremity rehabilitation". In Proceedings of the ASME International Design Engineering Technical Conferences and Computers and Information in Engineering Conference, Vol. 59179, American Society of Mechanical Engineers, p. V001T02A044.

[3] Yan, H., Yang, C., Zhang, Y., and Wang, Y., 2014. "Design and validation of a compatible 3-degrees of freedom shoulder exoskeleton with an adaptive center of rotation". *Journal of Mechanical Design,* **136**(7), p. 071006.

[4] Ghannadi, B., Razavian, R. S., and McPhee, J., 2018. "Upper extremity rehabilitation robots: A survey". In *Handbook of Biomechatronics*. Elsevier, ch. 9, pp. 319–353.

[5] Kiguchi, K., Iwami, K., Yasuda, M., Watanabe, K., and Fukuda, T., 2003. "An exoskeletal robot for human shoulder joint motion assist". *IEEE/ASME Transactions on Mechatronics,* **8**(1), pp. 125–135.

[6] Xu, K., Zhao, J., Qiu, D., and Wang, Y., 2014. "A pilot study of a continuum shoulder exoskeleton for anatomy adaptive assistances". *Journal of Mechanisms and Robotics,* **6**(4), p. 041011.

[7] Sylla, N., Bonnet, V., Colledani, F., and Fraisse, P., 2014. "Ergonomic contribution of ABLE exoskeleton in automotive industry". *International Journal of Industrial Ergonomics,* **44**(4), pp. 475–481.

[8] Otten, A., Voort, C., Stienen, A., Aarts, R., Van Asseldonk, E., and Van Der Kooij, H., 2015. "LIMPACT:A hydraulically powered self-aligning upper limb exoskeleton". *IEEE/ASME Transactions on Mechatronics,* **20**(5), pp. 2285–2298.

[9] Doyle, M. C., 2017. Adaptive Arm Support Systems and Methods for Use.

[10] Genani, G., 2018. Device with improved actuating means and method for use thereof, sep.

[11] Giovanelli, Y., and Vareille, A., 2018. "Dispositif d'assistance physique pour lutter contre les troubles musculosquelettiques". *Archives des Maladies Professionnelles et de l'Environnement,* **79**(3), p. 351.

[12] Van Engelhoven, L., Poon, N., Kazerooni, H., Ban, A., Rempel, D., and Harris-Adamson, C., 2018. "Evaluation of an adjustable support shoulder exoskeleton on static and dynamic overhead tasks". In Proceedings of the Human Factors and Ergonomics Society, Vol. 2, SAGE Publications, pp. 804–808.

[13] Angold, R., Lubin, J., Solano, M., Paretich, C., and Mastaler, T., 2016. Exoskeleton and method of providing an assistive torque to an arm of a wearer.

[14] Luque, E. P., Högberg, D., Iriondo, A., and Thorvald, P., 2019. "Evaluation of the use of exoskeletons in the range of motion of workers". Master thesis, University of Skövde.

[15] Gopura, R. A., Bandara, D. S., Kiguchi, K., and Mann, G. K., 2016. "Developments in hardware systems of active upper-limb exoskeleton robots: A review". *Robotics and Autonomous Systems,* **75**, pp. 203–220.

[16] Perry, J. C., Powell, J. M., and Rosen, J., 2009. "Isotropy of an upper limb exoskeleton and the kinematics and dynamics of the human arm". *Applied Bionics and Biomechanics,* **6**(2), pp. 175–191.

[17] Perry, J. C., Rosen, J., and Burns, S., 2007. "Upper-limb powered exoskeleton design". *IEEE/ASME Transactions on Mechatronics,* **12**(4), pp. 408–417.

[18] Galinski, D., Sapin, J., and Dehez, B., 2013. "Optimal design of an alignment-free two-DOF rehabilitation robot for the shoulder complex". In IEEE International Conference on Rehabilitation Robotics, IEEE, pp. 1–7.

[19] Manns, P., Sreenivasa, M., Millard, M., and Mombaur, K., 2017. "Motion optimization and parameter identification for a human and lower back exoskeleton model". *IEEE Robotics and Automation Letters,* **2**(3), pp. 1564–1570.

[20] Blanchet, L., Achiche, S., Docquier, Q., Fisette, P., and Raison, M., 2020. "A procedure to optimize the geometric and dynamic designs of assistive upper limb exoskeletons". *Multibody System Dynamics,* **51**(2), pp. 221–245.

[21] Shi, Y., and Peng, Q., 2018. "Improved benchmarking method using kinematics analysis in design of an upper limb exoskeleton rehabilitation device". In Proceedings of the ASME International Design Engineering Technical Conferences and Computers and Information in Engineering Conference, Vol. 4, American Society of Mechanical Engineers, p. V004T05A001.

[22] Sarac, M., Solazzi, M., Sotgiu, E., Bergamasco, M., and Frisoli, A., 2017. "Design and kinematic optimization of a novel underactuated robotic hand exoskeleton". *Meccanica,* **52**(3), pp. 749–761.

[23] Zhou, L., Li, Y., and Bai, S., 2017. "A human-centered design optimization approach for robotic exoskeletons through biomechanical simulation". *Robotics and Autonomous Systems,* **91**, pp. 337–347.

[24] Hayashi, Y., Dubey, R., and Kiguchi, K., 2011. "Torque optimization for a 7DOF upper-limb power-assist exoskeleton robot". In IEEE Workshop on Robotic Intelligence In Informationally Structured Space, IEEE, pp. 49–54.

[25] Aoustin, Y., and Formalskii, A. M., 2018. "Walking of biped with passive exoskeleton: evaluation of energy consumption". *Multibody System Dynamics,* **43**(1), pp. 71–96.

[26] Holzbaur, K. R., Murray, W. M., and Delp, S. L., 2005. "A model of the upper extremity for simulating

musculoskeletal surgery and analyzing neuromuscular control". *Annals of Biomedical Engineering,* **33**(6), pp. 829–840.

[27] Wu, G., Van Der Helm, F. C. T., Veeger, H. E. J., Makhsous, M., Van Roy, P., Anglin, C., Nagels, J., Karduna, A. R., McQuade, K., Wang, X. G., Werner, F. W., and Buchholz, B., 2005. "ISB recommendation on definitions of joint coordinate systems of various joints for the reporting of human joint motion - Part II: Shoulder, elbow, wrist and hand". *Journal of Biomechanics,* **38**(5), pp. 981–992.

[28] Dumas, R., Chèze, L., and Verriest, J. P., 2007. "Adjustments to McConville et al. and Young et al. body segment inertial parameters". *Journal of Biomechanics,* **40**(3), pp. 543–553.

[29] Naf, M. B., Junius, K., Rossini, M., Rodriguez-Guerrero, C., Vanderborght, B., and Lefeber, D., 2019. "Misalignment compensation for full human-exoskeleton kinematic compatibility: State of the art and evaluation". *Applied Mechanics Reviews,* **70**(5), p. 050802.

[30] Inkol, K. A., and McPhee, J., 2020. "Assessing control of fixed-support balance recovery in wearable lower-limb exoskeletons using multibody dynamic modelling". In Proceedings of the IEEE RAS and EMBS International Conference on Biomedical Robotics and Biomechatronics, Vol. 2020-Novem, IEEE, pp. 54–60.

[31] Garner, B. A., and Pandy, M. G., 2001. "Musculoskeletal model of the upper limb based on the visible human male dataset". *Computer methods in biomechanics and biomedical engineering,* **4**(2), pp. 93–126.

[32] Roetenberg, D., 2006. "Inertial and magnetic sensing of human motion". These de doctorat, University of Twente.

[33] Phadke, V., Braman, J. P., LaPrade, R. F., and Ludewig, P. M., 2011. "Comparison of glenohumeral motion using different rotation sequences". *Journal of Biomechanics,* **44**(4), pp. 700–705.

[34] McFarland, T. C., McDonald, A. C., Whittaker, R. L., Callaghan, J. P., and Dickerson, C. R., 2022. "Level of exoskeleton support influences shoulder elevation, external rotation and forearm pronation during simulated work tasks in females". *Applied Ergonomics,* **98**, p. 103591.

[35] Nasr, A., He, J., Jiang, N., and McPhee, J., 2020. "Activation torque estimation of muscles by forward neural networks (Forward-MuscleNET) for sEMG-based control of assistive robots". In Proceedings of the 7th International Conference of Control, Dynamic Systems, and Robotics (CDSR'20), p. 146.

[36] Nasr, A., and McPhee, J., 2020. "Control-oriented muscle torque (COMT) model for EMG-based control of assistive robots". In Proceedings of the 7th International Conference of Control, Dynamic Systems, and Robotics (CDSR'20), p. 144.

[37] Sone, J., Inoue, R., Yamada, K., Nagae, T., Fujita, K., and Sato, M., 2008. "Development of a wearable exoskeleton haptic interface device". *Journal of Computing and Information Science in Engineering,* **8**(4), pp. 0410091–04100912.

[38] Nasr, A., Laschowski, B., and McPhee, J., 2021. "Myoelectric control of robotic leg prostheses and exoskeletons: A review". In ASME 2021 Virtual International Design Engineering Technical Conferences & Computers and Information in Engineering Conference, ASME, pp. DETC2021–69203.

[39] Nasr, A., Bell, S., He, J., Whittaker, R. L., Jiang, N., Dickerson, C. R., and McPhee, J., 2021. "Muscle-NET: Mapping electromyography to kinematic and dynamic biomechanical variables". *Journal of Neural Engineering,* **18**(4), p. 0460d3.